Hopping conductivity of Ni-doped p-CdSb

2008 J. Phys.: Condens. Matter 20 295204

(http://iopscience.iop.org/0953-8984/20/29/295204)

J. Phys.: Condens. Matter **20** (2008) 295204 (8pp) doi:10.1088/0953-8984/20/29/295204

Hopping conductivity of Ni-doped p-CdSb

R Laiho[1], A V Lashkul[1,2], K G Lisunov[1,2,3], E Lähderanta[2], M A Shakhov[1,2,4] and V S Zakhvalinskii[1,5]

[1] Wihuri Physical Laboratory, University of Turku, FIN-20014 Turku, Finland
[2] Department of Physics and Mathematics, Lappeenranta University of Technology, FIN-53851 Lappeenranta, Finland
[3] Institute of Applied Physics, Academiei Str. 5, MD-2028 Kishinev, Moldova
[4] A F Ioffe Physico-Technical Institute, 194021 St Petersburg, Russia
[5] Department of Physics, Belgorod State University, RUS-308015 Belgorod, Russia

Received 7 January 2008, in final form 1 May 2008
Published 26 June 2008
Online at stacks.iop.org/JPhysCM/20/295204

Abstract

Mechanisms of the resistivity, ρ, of single crystal samples oriented along the [100] (No 1), [010] (No 2) and [001] (No 3) axes of anisotropic semiconductor p-CdSb doped with 2 at.% of Ni are investigated. In zero magnetic field the Mott type variable-range hopping (VRH) conductivity is observed in No 2 and the Shklovskii–Efros type in No 1 and No 3 at $T \leqslant 2.5$ K. The magnetoresistance (MR) of the samples obeys the law $\ln \rho \sim B^2$ up to $B \sim 6$ T. However, the temperature dependence of MR gives evidence for the Mott-VRH conductivity in No 1 at $T \leqslant 4.2$ K and the nearest-neighbor hopping conductivity in No 2 between $T = 3$ and 4.2 K and in No 3 between 1.5 and 4.2 K. From the experimental data the values of the localization radius and dielectric permittivity and details of their critical behavior near the metal–insulator transition, as well as the widths and the values of the density of the localized states, the acceptor energies, their concentrations and the anisotropy coefficients, are obtained.

(Some figures in this article are in colour only in the electronic version)

1. Introduction

Crystalline semiconductors doped with transition-metal elements can be divided into (i) compounds with microscopically homogeneous magnetization or semimagnetic semiconductors and (ii) diluted magnetic systems containing nanosize magnetic particles (clusters) and strongly inhomogeneous distribution of magnetization. Both groups of the materials exhibit spin-dependent electron transport [1].

Recently, magnetic properties of cadmium antimonide doped with Ni (p-CdSb:Ni) have been investigated [2]. The special interest in this compound is related to the strongly anisotropic transport properties of CdSb, which is a group II–V p-type semiconductor with orthorhombic crystal structure and the energy gap $E_g \sim 0.56$ eV at 0 K [3]. Undoped CdSb has non-degenerate charge carriers and activated conductivity governed by acceptor bands with energies $\sim$ 3 and 6 meV. Fe and Ni substituting for Sb in the lattice act as acceptors in CdSb. Doping with Ag induces in CdSb a metal–insulator transition (MIT) by removing the energy difference between the shallow acceptor states and the valence band [3]. Investigations of the Shubnikov–de Haas effect in heavily doped p-CdSb have yielded the values of the hole effective masses, $m_i = 0.16, 0.35$ and 0.19 (in units of free electron mass, m_0) in the crystallographic directions [100], [010] and [001], respectively [4]. On the metallic side of the MIT anisotropic quantum interference effects such as weak localization and anomalous magnetoresistance (MR) have been observed [5], whereas on the insulating side of the MIT anisotropic hopping conductivity was found [6].

Limited solubility of Ni in CdSb stimulates formation of a eutectic composition CdSb + NiSb at ~2 mol% of NiSb, containing needle-like NiSb inclusions of length $l \sim$ 30–40 μm and diameter $d \sim$ 1–1.5 μm [7]. On the other hand, at smaller doping level nanosize Ni-rich $Ni_{1-x}Sb_x$ ferromagnetic (FM) clusters are formed [2]. The clusters have a broad size distribution, high aspect ratio l/d and orientations distributed along a preferred direction. The presence of these clusters leads to considerable anisotropy of the magnetic properties of p-CdSb:Ni, as well as to a frustrated ground state and spin freezing below room temperature [2]. This makes p-CdSb:Ni a promising group (ii) material mentioned above.

Generally, galvanomagnetic properties of diluted magnetic semiconductors with itinerant electrons are investigated much better than those with localized charge carriers and hopping charge transfer. Moreover, investigations of the hopping

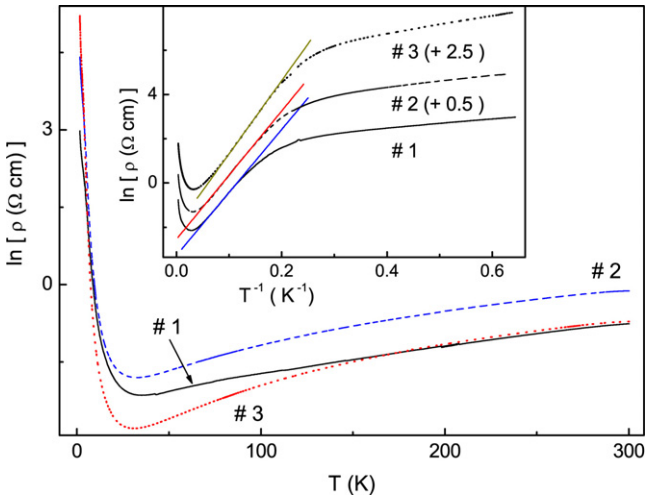

Figure 1. The temperature dependence of the resistivity of p-CdSb:Ni. Inset: plots of ln ρ versus T^{-1}. For convenience the data for No 2 and No 3 are shifted by +0.5 and +2.5 units along the vertical axis. The straight lines are linear fits.

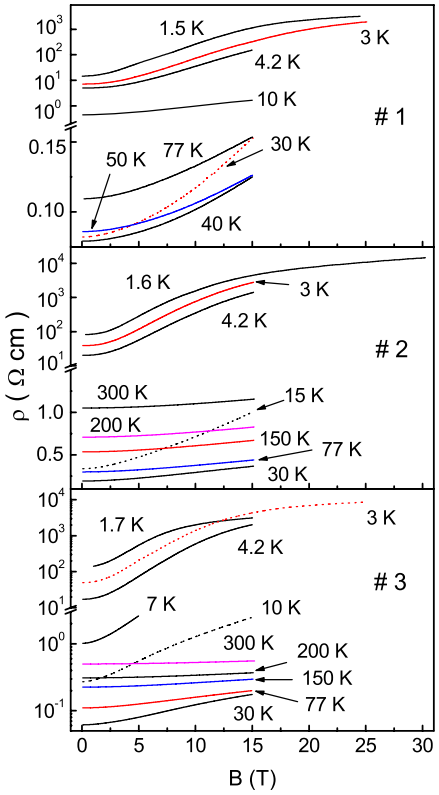

Figure 2. The dependence of the resistivity of p-CdSb:Ni on magnetic field.

conductivity in such compounds demonstrating anisotropic transport and magnetic behavior are lacking in the literature. On the other hand, in the group (ii) compounds one may expect new interesting features of hopping transport connected to inhomogeneous magnetization. The point is that hopping conduction mechanisms are determined strongly by the degree of internal microscopic disorder, whereas magnetic nanoclusters with broad size distribution bring to a system additional disorder of a magnetic nature, being sensitive to external magnetic field.

In this work we investigate the resistivity and MR of CdSb doped with Ni. Special attention is paid to the mechanisms of low-temperature charge transfer. Information about critical behavior of the microscopic parameters near the MIT and properties of localized charge carriers are obtained.

2. Experiment

Single crystals of CdSb doped with 2 at% of Ni were prepared by the modified Bridgman method [2]. As observed by x-ray diffraction, the ingots were of single phase material with orthorhombic structure (space group D_{2h}^{15}) and had the same lattice parameters as undoped CdSb. For investigations, rectangular prisms with the longest edge along the [100] (No 1), [010] (No 2) and [001] (No 3) axes, respectively, were cut from the ingots. The measurements of $\rho(T)$ were made by recording the signal from two different pairs of potential contacts on the samples placed in a He exchange gas Dewar, where their temperature could be varied between 1.5 and 300 K to an accuracy of 0.5%. MR measurements were made in transversal field configurations with $\boldsymbol{j} \parallel [100]$ and $\boldsymbol{B} \parallel [001]$ (No 1), $\boldsymbol{j} \parallel [010]$ and $\boldsymbol{B} \parallel [100]$ (No 2), $\boldsymbol{j} \parallel [001]$ and $\boldsymbol{B} \parallel [010]$ (No 3) at temperatures between $T = 1.5$ and 300 K in pulsed magnetic fields up to $B = 30$ T. The magnetic pulse length was 8 ms, the error in the strength of the field was not larger than 5% and its inhomogeneity did not exceed 0.3%. Measurements of the low-field Hall coefficient, R, at 77 K in fields below 0.1 T gave the Hall concentrations $p_{77} = (eR_{77})^{-1} = 3.56 \times 10^{16}$ cm^{-3}, 2.73×10^{16} cm^{-3} and 2.10×10^{16} cm^{-3} for No 1, 2 and 3, respectively.

As shown in figure 1 the values of $\rho(T)$ decrease smoothly below 300 K until a minimum is attained at ∼30 K followed by strong increase of ρ with further decreasing of T. The data of $\rho(B)$ in figure 2 show large positive MR, increasing with B and decreasing with increasing T at liquid He temperatures (approximately above the break in the $\rho(B)$ axis), whereas at higher T (below this break) the dependence of ρ on B is weakened. In addition, MR decreases with increasing T up to ∼30 K and then starts to increase, in agreement with the behavior of $\rho(T)$ at $B = 0$ shown in figure 1.

As can be seen from the inset to figure 1, the slopes of the plots of ln ρ versus T^{-1} exhibit two intervals of activated behavior characterized by different slopes between ∼5 and 20 K and below ∼5 K, which suggests the conductivity determined mainly by activation of the holes from shallow acceptor states to the valence band and the hopping conductivity over the states of the impurity band, respectively. The behavior of MR in figure 2, including a strong increase with B below ∼4.2 K followed by a weaker one above $T \sim$ 10 K, satisfies this conjecture, too (see below).

3. Theoretical background

The resistivity of a semiconductor in the interval of thermal activation of charge carriers from shallow impurity levels to

the conduction or valence band satisfies the law

$$\rho(T) = \rho_0 \exp[E_A/(kT)], \tag{1}$$

where ρ_0 is the prefactor and E_A is the activation energy [8]. On the other hand, the hopping conductivity in three-dimensional (3D) doped crystalline semiconductors can be realized via different mechanisms given by a universal equation

$$\rho(T) = DT^m \exp[(T_0/T)^p], \tag{2}$$

where D is a constant, T_0 is a characteristic temperature and $m = p$ for hydrogenic wavefunctions of the localized electrons, a case which is most expectable for doped crystalline semiconductors with shallow impurities at low temperatures [8] (although in other materials and temperature intervals the values of m may differ from p as discussed in detail in [9]). The case of $p = 1$ corresponds to the regime of nearest-neighbor hopping (NNH) conductivity and $p = 1/4$ and $1/2$ to the Mott [10] and the Shklovskii–Efros (SE) [8] types of variable-range hopping (VRH) conductivity, respectively. Generally, the VRH conductivity sets in when the internal microscopic disorder is high enough to make tunneling between the nearest sites energetically unfavorable. Because at low T hopping of the electrons takes place only within a limited energy interval or the Mott's optimum energy stripe $\Delta\varepsilon\ (T)$ around the Fermi level, μ [10], the type of the VRH charge transfer depends on the relations between $\Delta\varepsilon\ (T)$ (decreasing with T), the width W of the impurity band or density of the localized state (DOS), $g(\varepsilon)$, and the width Δ of the parabolic Coulomb gap, which exists around μ due to the Coulomb interaction between the charge carriers in disordered materials [8]. The general result is that for $\Delta < \Delta\varepsilon(T) < W$ and weak dependence of $g(\varepsilon)$ the Mott-VRH conductivity sets in, whereas for $\Delta\varepsilon(T) < \Delta$ the VRH conductivity is of the SE type [8, 10]. Hence, the temperature interval where one out of the two types of VRH conductivity dominates depends on the relation between Δ and W, both being sensitive to the degree of disorder: the higher ratio of Δ/W favors the SE-VRH conductivity at higher T, whereas the lower Δ/W stimulates the Mott-VRH, shifting the onset of the SE-VRH conductivity to lower T.

The characteristic temperature in the case of the Mott- and SE-VRH conductivity mechanisms can be written as

$$T_{0M} = \beta_M/[kg(\mu)a^3], \qquad T_{0SE} = \beta_{SE}e^2/(k\kappa a) \tag{3}$$

respectively, where κ is the dielectric permittivity, $\beta_M = 21$, $\beta_{SE} = 2.8$ and $a = (a_1a_2a_3)^{1/3}$ is the mean localization radius [8]. Here a_i ($i = 1, 2$ and 3) scales the exponential decay of the anisotropic impurity wavefunctions (which takes place in p-CdSb as well—see the introduction) in the ith direction, where the anisotropy of a_i is connected to that of m_i as follows: for $N_A \ll N_C$ (far from MIT) $a_i = a_{0i} \equiv \hbar(2m_iE_A)^{-1/2}$ and for $N_A \to N_C$ (close to the MIT) $a_i = a_{0i}(1 - N_A/N_C)^\nu$, where N_A and N_C are the impurity concentration (acceptor concentration in the case of p-CdSb) and the critical concentration of MIT, respectively, and ν is the critical exponent of the correlation length [8, 10, 11]. One can also introduce the mean parameter $a_0 \equiv (a_{01}a_{02}a_{03})^{1/3}$ to obtain a general expression

$$a = a_0(1 - N_A/N_C)^\nu, \tag{4}$$

the same as in an isotropic material [11].

To find the regime of hopping conductivity at $B = 0$ it is convenient to rewrite equation (2) as

$$\ln[E_a/(kT) + m] = \ln p + p \ln T_0 + p \ln(1/T), \tag{5}$$

where $E_a \equiv \mathrm{d}\ln\rho/\mathrm{d}(kT)^{-1}$ is the *local activation energy* [8], so that for a certain conductivity mechanism the left-hand side of equation (5) would be a linear function of $\ln(1/T)$ and p would be given by the slope of the plot $\ln[E_a/(kT)+m]$ versus $\ln(1/T)$.

In weak fields with magnetic length $\lambda \gg a_0$ quadratic dependence of $\ln\rho$ on B has been predicted for all the mechanisms of the hopping conductivity considered above. The positive MR is connected to shrinkage of the impurity wavefunctions in the direction perpendicular to $\boldsymbol{B}$ [8, 12]. On the other hand, the dependence of $\ln\rho(B)$ on temperature is different for each hopping regime. Namely, for the NNH conductivity we get

$$\ln[\rho(B)/\rho(0)]_j = C_jB^2, \tag{6}$$

where the prefactor

$$C_j = te^2ap_j^2/(\hbar^2N_A) \tag{7}$$

does not depend on T. Here $t = 0.036$ [8] and

$$p_j = [m_j^2/(m_km_l)]^{1/6} \tag{8}$$

is the anisotropy coefficient [6], with $j, k, l = 1, 2, 3$ ($j \neq k \neq l$) and $j = 3, 1, 2$ for No 1, No 2 and No 3, respectively, corresponding to the direction of the *magnetic field* along the [001], [100] and [010] axes, respectively. In equation (7) p_j reflects the different elasticity of the anisotropic acceptor wavefunctions to magnetic shrinkage at different directions of $\boldsymbol{B}$ [6, 8].

As in the case of the NNH conductivity [6], it can be shown that for the Mott-VRH conductivity in low fields one gets an expression similar to equation (6), but with C_j replaced by $A_j^{(M)}(T) = A_{0j}^{(M)}T^{-3/4}$, where

$$A_{0j}^{(M)} = t_1e^2a^4T_{0M}^{3/4}p_j^2/\hbar^2 \tag{9}$$

and $t_1 = 5/2016$ [8] with the meanings and the values of p_j and j the same as in equations (6)–(8). Finally, for the SE-VRH conductivity in low fields, instead of C_j in equation (6) we have $A_j^{(SE)}(T) = A_{0j}^{(SE)}T^{-3/2}$, where $A_{0j}^{(SE)}$ is given by an expression similar to equation (9) but with $t_2 = 0.0015$ and T_{0SE} instead of t_1 and T_{0M}, respectively [12].

Finally, it is worth mentioning at this point that damping of the quantum interference of hopping electrons in the magnetic field leads to the negative magnetoresistance (NMR) in the VRH conductivity regime of doped semiconductors [13].

Table 1. The values of the prefactor (ρ_0) and the activation energy (E_A) in the acceptor freeze-out interval and the prefactor constant (D) and the characteristic temperature of the VRH conductivity (T_0) in the hopping conductivity interval at $B = 0$.

Sample No	ρ_0 (Ω cm)	E_A (meV)	D (Ω cm K^{-p})	T_0 (K)
1	0.0378	2.45	0.491[a]	18.7[a]
2	0.0475	2.50	0.0928[b]	3180[b]
3	0.0111	2.85	0.477[a]	51.3[a]

[a] $p = 1/2$ (SE-VRH regime).
[b] $p = 1/4$ (Mott-VRH regime).

It has been predicted that for non-interacting electrons NMR dominates in low fields of $B < B_0$, where $B_0 \approx 1.3B^*$ and

$$B^* = \frac{4\hbar c}{a^2 e}\left(\frac{T}{T_{0M}}\right)^{3/8}, \qquad (10)$$

if both field effects, on the quantum interference and on the impurity wavefunctions (leading to PMR—see above), are taken into account simultaneously. In the opposite case of $B > B_0$ MR is positive and at $B = B_0$ it changes sign [14].

4. Analysis of the experimental data

4.1. Resistivity in zero magnetic field

The activation energy E_A connected to thermal excitation of the holes to the valence band can be obtained by fitting of the plots of $\ln\rho$ versus T^{-1} with equation (1) between ~5 and 20 K (the straight lines in the inset of figure 1) provided that the prefactor ρ_0 depends only weakly on T. The values of E_A are collected in table 1. However, neglecting the temperature dependence of ρ_0 only approximate values of E_A can be found due to temperature dependence of the hole mobility.

Analysis of the hopping conductivity can be done as follows. At first, putting $m = 1/2$ we obtain with equation (6) the values of p close to 1/2 in No 1 and No 3, which is characteristic of the SE-VRH conductivity regime below the temperature $T_v \approx 2.5$ K (see the top panel of figure 3). However, in No 2 the situation is quite different: putting $m = 1/4$ we find with equation (6) that $p \approx 1/4$ between $T_v \approx 2.5$ K and $T' \approx 1.8$ K, whereas below T' the left-hand side of equation (6) exhibits a systematic decrease, which takes place at $m = 0$ as well. The behavior of the local activation energy in the interval of (T_v, T') is typical of the Mott-VRH conductivity. On the other hand, the decrease of the left-hand side of equation (6) below T' is attributable to an intermediate region between the Mott- and the SE-VRH conductivity regimes (similar to the descending branch above T_v which corresponds to the intermediate interval between the band conduction and the hopping conduction), provided that the onset temperature of the latter lies below ~1.6 K. We will return to this conjecture further in section 5. Next, we plot $\ln(\rho/T^{1/2})$ versus $T^{-1/2}$ in the middle panel of figure 3 for all samples and $\ln(\rho/T^{1/4})$ versus $T^{-1/4}$ in the bottom panel of figure 3 for No 2. Comparing these plots, one can find a broader linear interval of the low-temperature

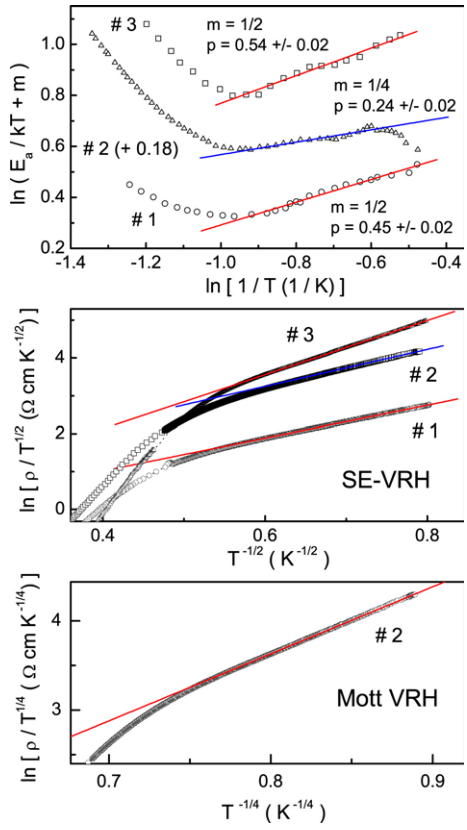

Figure 3. Plots of $\ln(E_a/kT + m)$ versus $\ln(1/T)$ (top panel), $\ln(\rho/T^{-1/2})$ versus $T^{-1/2}$ (middle panel) and $\ln(\rho/T^{-1/4})$ versus $T^{-1/4}$ (bottom panel). For convenience the data for No 2 on the top panel are shifted along the vertical axis by +0.17 units. The lines are linear fits.

data for No 1 and No 3 than for No 2 in the middle panel of figure 3, as well as expansion of this interval for No 2 in the bottom panel of figure 3. According to equation (2) this supports completely the identification of the hopping conductivity regimes followed from the top panel of figure 3. Hence, the SE-VRH conductivity is realized in No 1 and No 3 and the Mott-VRH conductivity in No 2, whereas no intervals of the NNH conductivity are observed. The values of D, T_{0SE}, T_{0M} are found from the plots in the middle and bottom panels of figure 3 and are collected in table 1.

It is important to note at this point that at first glance the interval of the hopping conduction above looks rather small to identify the mechanisms of the hopping charge transfer in zero magnetic field. However, this has been done based on the analysis of the resistivity *with two different methods* including those shown in the top panel of figure 3 and on the middle and bottom panels of figure 3. Both methods yield unambiguous conclusions on the mechanism of the hopping conductivity and *give the same VRH conduction regime* for one and the same sample.

Finally, we discuss the role of the prefactor in equation (2) and the importance of its temperature dependence given by the exponent m. Many authors in analysis of hopping conductivity with equation (2) neglect this point by putting $m = 0$, which is completely substantiated when $\rho(T)$ changes by several

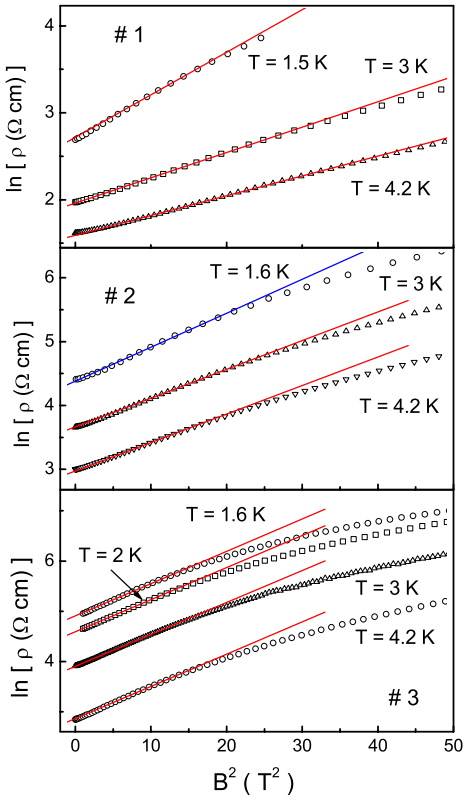

Figure 4. Plots of $\ln \rho$ versus B^2. The lines are linear fits to the experimental data.

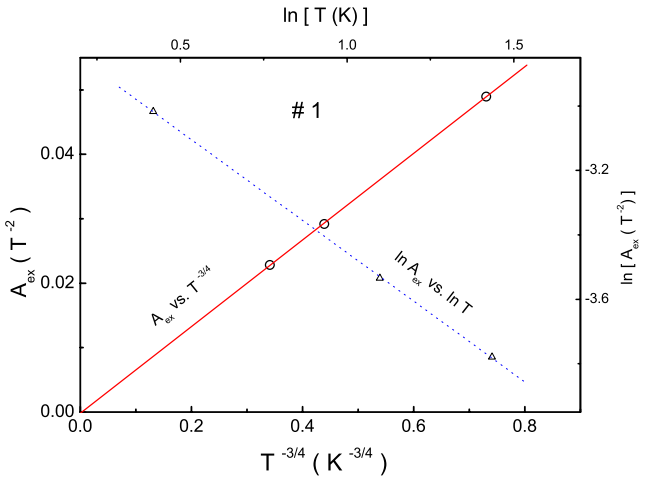

Figure 5. The dependences of $A_{\rm ex}$ on $T^{-3/4}$ (O) and of $\ln A_{\rm ex}$ on $\ln T$ (Δ) for No 1. The lines are linear fits.

orders of magnitude, making the relatively weak power-law temperature dependence of the prefactor unimportant with respect to the much stronger exponential one. However, this may not be so when the dependence $\rho(T)$ is not strong enough. As can be seen in figure 1 (inset), in the interval of hopping conductivity $\rho(T)$ varies only a few-fold, definitely within one order of magnitude, and the temperature dependence of the prefactor should be taken into account. To clarify this issue we analyzed the same plots as in figure 3 but with $m = 0$, yielding the following results: (i) from the plots of $\ln(E_{\rm a}/kT)$ versus $\ln(1/T)$ the values of $p = 0.44 \pm 0.02$, 0.26 ± 0.02 and 0.62 ± 0.04 are obtained for No 1, No 2 and No 3, respectively, and (ii) from the plots of $\ln \rho$ versus $T^{-1/2}$ and $\ln \rho$ versus $T^{-1/4}$ the values of $T_0 = 8.7$ K, 1590 K and 33.9 K are obtained for No 1, No 2 and No 3, respectively. On one hand, it can be seen that neglect of the temperature dependence of the prefactor in equation (1) causes only small differences in p following from the analysis of the local activation energy, which cannot spoil the identification of the VRH conductivity mechanisms above (in fact, even in the worst case of No 3 the value of $p = 0.62$ is much closer to $1/2$ than to other possible values in 3D doped crystalline semiconductors, $1/4$ and 1 [8, 10]). On the other hand, the differences of T_0 are very large (up to twofold—cf table 1), which in turn would lead to more serious errors in subsequent analysis involving this parameter.

4.2. Resistivity in weak magnetic fields

As can be seen from figure 4 the plots of $\ln \rho$ versus B^2 below $B \sim 6$ T can be approximated well with linear functions, which is in agreement with equation (6). Slight deviations from linearity are observed for No 1 and No 2 only in the weakest fields. These deviations are attributable to a small negative contribution to MR (see the end of section 3), which will be verified in more detail in section 5. In No 3 the slope of the plots is $C_{\rm ex}^{(3)} = (6.41 \pm 0.04) \times 10^{-2} T^{-2}$ between 1.6 and 4.2 K. The slope of the corresponding plots for No 2, $C_{\rm ex}^{(2)} = (4.49 \pm 0.04) \times 10^{-2} T^{-2}$, does not vary between 3 and 4.2 K and it increases only slightly between 3 and 1.6 K. In sample No 1 all the plots have different slopes varying with T according to the function $A_{\rm ex}(T) = A_{\rm ex}^{(0)} T^{-3/4}$ with $A_{\rm ex}^{(0)} = (6.7 \pm 0.1) \times 10^{-2} T^{-2}$ K$^{3/4}$ as shown in figure 5.

Hence, from comparison of the behavior of the slopes of the plots of $\ln \rho$ versus B^2, $C_{\rm ex}^{(2)}$, $C_{\rm ex}^{(3)}$ and $A_{\rm ex}(T)$ with C_j, $A_j^{\rm (M)}(T)$ and $A_j^{\rm (SE)}(T)$, predicted for the different hopping regimes (see section 3, equations (7), (9) and remarks to equation (9)), it follows that, in contrast to the case of $B = 0$, in No 1 the Mott-VRH conductivity takes place between 1.6 and 4.2 K, in No 2 the NNH conductivity is observed between 3 and 4.2 K and in No 3 the NNH conductivity is realized within the whole temperature interval between 1.6 and 4.2 K.

4.3. Determination of the microscopic parameters

The data at $B = 0$ and in weak fields obtained above allow determination of a variety of microscopic parameters for verification of the conclusions about the mechanisms of hopping conductivity made above. This will be done in steps (i)–(viii) below.

(i) With the expression

$$\Delta \approx 0.5k(T_{\rm VSE}T_{\rm 0SE})^{1/2} \tag{11}$$

the width of the Coulomb gap for No 1 can be determined [8]. Then from the equation $\Delta \approx U$,

Table 2. The acceptor concentration (N_A), the localization radius (a), the dielectric permittivity (κ), the widths of the Coulomb gap (Δ) and of the acceptor band (W), the density of the localized states (g) and the experimental (p_j) and the calculated ($p_j^{(cal)}$) values of the anisotropy coefficients at different orientations of the magnetic field (j).

Sample No.	N_A (10^{16} cm^{-3})	a (Å)	κ	Δ (meV)	W (meV)	g (10^{16} cm^{-3} meV^{-1})	p_j	$p_j^{(cal)}$	j
1	3.61	196	127	0.30	0.50	5.94	0.839	0.839	3
2	3.37	180	108	0.18[a]	1.28	1.31	1.008	0.897	1
3	2.51	139	66	0.49	0.91	2.16	1.182	1.327	2

[a] Calculated.

where $U = e^2/(\kappa R_h)$ is the energy of the Coulomb repulsion between the holes at the mean distance $R_h \approx 2(4\pi p_{77}/3)^{-1/3}$, the value of κ can be found. Here we use the values of p_{77} (section 2), taking into account that the shallow acceptor states at $E_A \sim 2.4$–2.8 meV above the top of the valence band are completely ionized at 77 K. The value of DOS outside the Coulomb gap, g_0, can be evaluated with the expression $g_0 = 3\kappa^3\Delta^2/(\pi e^6)$ [8]. Usually the DOS parameters in the Mott-VRH and the SE-VRH models, $g(\mu)$ and g_0, are close to each other in doped semiconductors (see e.g. [15]), and so T_{0M} can be calculated with the first of equations (3) at $g(\mu) \approx g_0 \equiv g$. Finally, with equation (9) we obtain for $A_{03}^{(M)} = A_{ex}^{(0)}$ the anisotropy coefficient p_3 ($j = 3$ for No 1). The values of Δ, κ, a, g and p_3 for No 1 are collected in table 2.

(ii) The parameters Δ, κ, a and $g_0 \equiv g$ for No 3 can be found as in (i). Their values are given in table 2.

(iii) The values of a for No 1 and No 3 exceed by 2.1–2.9 times the Bohr radius, $a_B = \hbar^2\kappa_0/(me^2) = 66.8$ Å, where $m = (m_1m_2m_3)^{1/3} = 0.20$ and $\kappa_0 \approx 25$ is the value of κ far from the MIT [16]. The values of κ exceed that of κ_0 by 2.6–5.1 times. Taking into account equation (4) and a similar expression

$$\kappa = \kappa_0(1 - N_A/N_C)^{-\zeta} \qquad (4')$$

where ζ is the critical exponent of κ [11], the enhanced values of a and κ are consistent with proximity to the MIT, N_A being relatively close to N_C. Then with equations (4) and (4′) one gets the relation

$$\frac{\zeta}{\nu} = \frac{\ln\left[\kappa(\text{No 1})/\kappa(\text{No 3})\right]}{\ln\left[a(\text{No 1})/a(\text{No 3})\right]}, \qquad (4'')$$

yielding $\zeta/\nu = 1.90$. On the other hand, from equations (4) and (4′) we have a pair of equations $a_0 = a(\text{No 1})[\kappa_0/\kappa(\text{No 1})]^{\nu/\zeta}$ and $a_0 = a(\text{No 3})[\kappa_0/\kappa(\text{No 3})]^{\nu/\zeta}$, giving the same value of the mean localization radius $a_0 = 83.5$ Å far from the MIT. Finally, with the equation $E_A = \hbar^2/(2ma_0^2)$ (see text between equations (3) and (4) in section 3) we obtain $E_A = 2.78$ meV.

(iv) Suppose that the value of p_2 is known. Then with equation (7) at $C_2 = C_{ex}^{(3)}$ ($j = 2$ for No 3) the value of N_A for No 3 can be evaluated. It can be shown that for a rectangular DOS having the Coulomb gap at the Fermi level the width W of the DOS (or the width of the acceptor band) is given by the equation

$$W = \frac{N_A}{2g_0} + \frac{2}{3}\Delta, \qquad (12)$$

allowing evaluation of W for No 3.

(v) In No 2 the influence of the Coulomb gap is minimal since only the Mott-VRH conductivity is realized at $B = 0$. Therefore the DOS in the acceptor band can be approximated with a rectangular shape without including Δ and we get $W \approx kT_{VM}^{3/4}T_{0M}^{1/4}$ for this sample [8]. Then, using the relation $p_1 = (p_2p_3)^{-1}$ following from equation (8) and the expression $g(\mu) \approx N_A/(2W)$ valid for this choice of the DOS, and solving equations (3) and (7) with $C_1 = C_{ex}^{(2)}$ (note that $j = 1$ for No 2), the values of a and N_A can be obtained. After N_A is known, the value of $g(\mu) \equiv g$ can be determined.

(vi) The value of ν can be calculated with the expression

$$\nu = \ln\left[\frac{1 - a_0/a(\text{No 3})}{1 - a_0/a(\text{No 2})}\right] \times \left\{\ln\left[\frac{N_A(\text{No 3})}{N_A(\text{No 2})}\right]\right\}^{-1} \qquad (13)$$

following from equation (4). Then N_C can be found with the equations

$$\begin{aligned} N_C &= N_A(\text{No 2})[1 - a_0/a(\text{No 2})]^{-1/\nu}, \\ N_C &= N_A(\text{No 3})[1 - a_0/a(\text{No 3})]^{-1/\nu}. \end{aligned} \qquad (14)$$

Using the values of ν and the ratio ζ/ν obtained above we get ζ and

$$\kappa^{(cal)}(\text{No 3}) = \kappa_0[1 - N_A(\text{No 3})/N_C]^{-\zeta}. \qquad (15)$$

Steps (iv)–(vi) are repeated by variation of p_2 until the values of N_C in equations (14) coincide and, additionally, the condition $\kappa^{(cal)}(\text{No 3}) = \kappa(\text{No 3})$ is satisfied. This gives $\nu = 1.00$, $\zeta = 1.90$, $N_C = 6.275 \times 10^{16}$ cm^{-3}, $N_C^{1/3}a_B = 0.265$, and yields the values of p_1 and p_2 in table 2.

(vii) Knowing ν, ζ, a_0 and κ_0, one can evaluate N_A for No 1 with any of the equations (4) and (4′) yielding the same result. Then W can be obtained with equation (12) (because in No 1 the effect of the Coulomb gap cannot be neglected), using the data of $g_0 \equiv g$ and Δ determined in step (i) (table 2).

(viii) With N_C and ζ found in (iv)–(vi) and κ_0 and N_A in No 2 evaluated in (v), the value of κ can be obtained

from equation (4′). Then from the expression $g_0 = 3\kappa^3\Delta^2/(\pi e^6)$ [8] at $g_0 \approx g(\mu)$ in (v) the value of Δ can be calculated. The parameters κ and Δ for No 2 are given in table 2. Finally, from the second of equations (3) we evaluate T_{0SE} and from equation (11) $T_{VSE} \approx 4\Delta^2/(T_{0SE}k^2) \approx 0.7$ K in No 2. The parameters N_A, K and W for all samples are obtained in (iv)–(vii). The values of $g(\mu) \equiv g$ and a found for No 2 in step (v) are given in table 2.

5. Discussion

The relations of the obtained microscopic parameters in table 2, $a(\text{No 1}) > a(\text{No 2}) > a(\text{No 3})$ and $\kappa(\text{No 1}) > \kappa(\text{No 2}) > \kappa(\text{No 3})$, are in line with the corresponding relation $N_A(\text{No 1}) > N_A(\text{No 2}) > N_A(\text{No 3})$, where the values of N_A are relatively close to N_C. Such dependence agrees well with the proximity of the acceptor system in p-CdSb:Ni to the MIT, and the critical exponents found in steps (iv)–(vi) are close to their theoretical values $\nu = 1$ and $\zeta = 2$ [11]. The value of the product $N_C^{1/3}a_B = 0.265$ obtained in section 4.3 after steps (iv)–(vi) agrees well with the Mott criterion $N_C^{1/3}a_B \approx 0.25$ [10] for the critical concentration at the MIT, and the value of the shallow acceptor energy $E_A \approx 2.78$ meV evaluated with a_0 found in step (iii) agrees reasonably with the corresponding data within the temperature interval of the acceptor freeze-out in figure 1 (table 1).

Next, the anisotropy coefficients satisfying the condition $p_2 > p_1 > p_3$, as may be expected for p-CdSb, can be compared with those calculated with equation (8) using the data of m_i cited in section 1 (see table 2), and yielding coincidence of p_3 and $p_3^{(cal)}$ and a difference of ∼11% between the other two pairs. At this point, we must note that p_3 was determined in section 4.3 in a most direct way in step (i), whereas p_1 and p_2 were obtained with a less direct procedure, (iv)–(vi), which may contain additional sources of errors. On the other hand, the valence band of CdSb is non-parabolic [4], and, strictly speaking, we should compare our data of p_j with those evaluated using the values of m_i at the top on the valence band, which differ somewhat from those determined at the Fermi energy from the Shubnikov–de Haas effect [4]. Taking this into account the difference between the experimental and the calculated values of p_1 and p_2 does not look too large. Hence, the anisotropy of hopping conductivity in p-CdSb:Ni is well described by the anisotropy of the hole effective mass, which occurs in undoped p-CdSb as well [6].

The relations between the values of Δ and W (concerning the role of the ratio of Δ/W in the VRH conduction mechanism see section 3) agree with the types of VRH conductivity observed at $B = 0$ in each sample. Indeed, in No 1 and No 3 the Coulomb gap has about half the width of the acceptor band stimulating the SE-VRH conductivity regime, whereas the ratio of $\Delta/W \sim 0.1$ in No 2 is more favorable for the Mott-VRH conductivity in the same temperature interval, so that the onset of the conductivity over the states of the Coulomb gap in No 2, estimated at the end of section 4.3 ($T_{VSE} \approx 0.7$ K), lies outside the temperature interval down to ∼1.6 K used in the measurements of $\rho(T)$. This supports our conjecture that the decrease of the left-hand side of equation (6) with decreasing T between ∼1.8 and 1.6 K may mean the existence of an intermediate interval between the Mott- and the SE-VRH conductivity regimes (see section 4.1 and the top panel of figure 3, where $T = 1.6$ K corresponds to the right edge of the abscissa axis). At this point we must underline that observation of the Mott- or the SE-VRH conductivity in different directions of p-CdSb:Ni at $B = 0$ is not connected immediately to the intrinsic anisotropy of p-CdSb, but mostly to correlation between Δ and W, which eventually depends on internal microscopic disorder being different in all samples cut from different parts of the ingot.

Above we have supposed that slight deviations of the plots in the top and middle panels of figure 4 from linearity in the weakest fields may be due to the negative contribution to MR, connected to the quantum interference of hopping electrons (see section 4.2). As mentioned in section 3, such NMR is expected to be important at $B < B_0$, where $B_0 \approx 1.3B^*$ and B^* is given by equation (10). A scale of B_0 can be estimated for No 2, taking $T = T_v \approx 2.5$ K and the values of T_{0M} and a from tables 1 and 2, respectively. This yields $B_0 \approx 0.7$ T, which is in agreement with the fields where deviations from linearity of the plots in figure 4 are observed. Therefore, a contribution of interference effects to MR can be important only for B covering a negligible part of the field interval used in our analysis.

Hence, the set of the microscopic parameters determined from the resistivity data at $B = 0$ and in weak magnetic fields, is consistent and supports the conclusions about the hopping conductivity mechanisms made from the temperature dependences of ρ and MR in sections 4.1 and 4.2, respectively. On the other hand, one can see that the hopping conductivity in p-CdSb:Ni contains features not common to conventional (non-magnetic) doped semiconductors. Namely, the VRH conductivity at $B = 0$ transforms into the NNH conductivity at $B \neq 0$ in No 2 and No 3 (or the type of the VRH conductivity is changed in No 1), which is accompanied by an increase of the onset temperature of the hopping conductivity from ∼2.5 K in zero field up to at least 4.2 K in non-zero field (cf figures 3 and 5).

In conventional semiconductors the type of the hopping conductivity is insensitive to magnetic field, whereas the broadening of the temperature interval of the hopping conductivity can be expected only in strong magnetic fields $B > B_0$, where $B_0 = \hbar/(ea_0^2) \approx 10$ T is the field where the magnetic length λ reaches a_0, and deviations from the dependence of $\ln\rho \sim B^2$ are observed. This leads to the onset of the magnetic field dependence of E_A, stimulating the acceptor freeze-out with increasing field [8], which favors hopping conductivity and has been observed in undoped p-CdSb [6], but cannot take place in our case of low fields $B < 6$ T in the interval of the quadratic dependence of MR [8].

Besides the charge and lattice disorders typical of non-magnetic doped semiconductors, p-CdSb:Ni, belonging to group (ii) of the diluted magnetic materials (see the introduction), also possesses magnetic disorder due to strongly inhomogeneous magnetization or the presence of small Ni-rich clusters with FM ordering of internal spins and broad

distribution of the cluster size [2]. In particular, this leads to magnetic irreversibility or deviation of zero-field cooled magnetic susceptibility, χ_{ZFC}, from field cooled susceptibility, χ_{FC}, in weak fields and the appearance of a broad maximum of $\chi_{ZFC}(T)$, reflecting spin-freezing phenomena with onset near room temperature [2]. Therefore, if the inhomogeneity of the local magnetization, caused by randomly frozen-in cluster moments, is significant within the average distance between the acceptors, the interaction of the spins of the carriers with local magnetic moments would be different already for nearest sites. This would create an additional energy barrier ΔE at $B = 0$ hindering tunneling of the carriers between the nearest sites in favor of VRH conductivity. However, in p-CdSb:Ni the magnetic disorder is damped already at $B \sim 0.4$ T by orienting magnetic moments of the clusters along the field [2]. Therefore, ΔE is decreased in the field stimulating the NNH conductivity. This mechanism should be more significant at low temperatures, where the fraction of the frozen-in spins is higher, i.e. in the interval of the hopping conductivity, in agreement with the unusual sequence of the hopping conductivity regimes observed in p-CdSb:Ni. In addition, damping of magnetic disorder stimulates the hopping conductivity in general, favoring tunneling of the electrons between any sites, which increases its efficiency over the band mechanism (activation of the holes into the valence band) at higher temperatures. This may explain the expansion of the interval of the hopping conductivity already in low fields.

6. Conclusions

We have investigated the resistivity and magnetoresistance of p-CdSb doped with 2 at% Ni. The resistivity at $B = 0$ exhibits activated behavior with two temperature intervals, one where the conductivity is governed by activation of holes to the valence band at T between ∼5 and 20 K and the other realized by hopping charge transfer at temperatures below $T_v \sim 2.5$ K. The variable-range hopping conductivity of the Mott or the Shklovskii–Efros types is observed at $B = 0$. In fields up to ∼6 T the resistivity obeys the law $\ln \rho \sim B^2$, whereas the temperature dependence of the magnetoresistance gives evidence for variable-range hopping conductivity of the Mott type or the nearest-neighbor hopping conductivity. The values of the microscopic parameters such as the localization radius, the dielectric permittivity, the widths and the values of the density of the localized states, the acceptor energies and concentrations and the anisotropy coefficients, obtained from the analysis of the resistivity and the magnetoresistance data, support identification of the hopping regimes in the intervals of the magnetic field concerned above. The tendency of transformation of the dominating charge transfer from variable-range hopping to nearest-neighbor hopping with increasing B can be attributed to the intrinsic magnetic disorder in p-CdSb:Ni.

References

[1] Žutić I, Fabian J and Das Sarma S 2004 *Rev. Mod. Phys.* **76** 323
[2] Laiho R, Lashkul A V, Lisunov K G, Lähderanta E, Ojala I and Zakhvalinskii V S 2006 *Semicond. Sci. Technol.* **21** 228
[3] Arushanov E K 1986 *Prog. Cryst. Growth Charact.* **13** 1
[4] Arushanov E K, Lashkul A V, Pruglo V I, Radautsan S I and Sologub V V 1982 *Sov. Phys.—Dokl.* **27** 3
[5] Arushanov E K, Lashkul A V, Lisunov K G, Parfen'ev R V and Radautsan S I 1987 *Sov. Phys.—Solid State* **29** 1450
[6] Laiho R, Lashkul A V, Lisunov K G, Lähderanta E, Safonchik M O and Shakhov M A 2004 *J. Phys.: Condens. Matter* **16** 333
[7] Marenkin S F, Saidullaeva M, Sanygin V P and Kovaleva I S 1982 *Izv. Akad. Nauk SSSR, Neorg. Mater.* **18** 1759
[8] Shklovskii B I and Efros A L 1984 *Electronic Properties of Doped Semiconductors* (Berlin: Springer)
[9] Laiho R, Lisunov K G, Lähderanta E, Petrenko P A, Salminen J, Shakhov M A, Safontchik M O, Stamov V S, Shubnikov M V and Zakhvalinskii V S 2002 *J. Phys.: Condens. Matter* **14** 8043
[10] Mott N F and Davies E A 1979 *Electron Processes in Non-Crystalline Materials* (Oxford: Clarendon)
[11] Castner T G 1991 *Hopping Transport in Solid* ed M Pollak and B Shklovskii (Amsterdam: Elsevier) p 3
[12] Shklovskii B I 1983 *Sov. Phys.—Semicond.* **17** 1311
[13] Shklovskii B I and Spivak B Z 1991 *Hopping Transport in Solid* ed M Pollak and B Shklovskii (Amsterdam: Elsevier) p 271
[14] Raikh M E and Wessels G F 1993 *Phys. Rev.* B **47** 15 609
[15] Arushanov E, Lisunov K G, Vinzelberg H, Behr G and Schumann J 2006 *J. Appl. Phys.* **100** 113704
[16] Borets A M, Rarenko I M and Rusnak V V 1984 *Proc. 6th All-Union Joint Conf. on Materials Science of II–V Semiconductor Compounds* (Moscow: IONH) p 108